JOURNAL OF Applied Polymer SCIENCE

Evaluation of typical rheological models fitting for polycarbonate squeeze flow

Wei Cao,[1] Tao Wang,[2] Yue Yan,[2] Yanhui Qi,[1] Shixun Zhang,[1] Qian Li,[1] Changyu Shen[1]

[1]Engineering Research Center of Mold and Die, Zhengzhou University, Zhengzhou, Henan Province, China

[2]Beijing Institute of Aeronautical Materials, Beijing, China

Correspondence to: W. Cao (E-mail: wcao@zzu.edu.cn)

ABSTRACT: High viscous polycarbonate melt exhibits some special rheological characters different from generalized Newtonian fluid during squeezing. It is necessary to evaluate whether the typical rheological models are suitable for polycarbonate squeeze. To avoid the difficult of measuring the inner melt rheological behavior directly, this study presents a method of measuring the compressing force applied on the upper disc of the rheometer to reveal the melt rheology indirectly. The finite difference method (FDM) was employed to discretize the governing equations and constitutive equations established on cylinder coordinate system and to simulate the compressing force. The experiments were carried out under four temperatures and three compressing velocities to test the validations of Leonov, Phan-Thien–Tanner (PTT), eXtended Pom-Pom (XPP), and Cross Williams–Landel–Ferry (Cross-WLF) models. The experimental results show the unique character of compressing force evolution as 'steep—steady—steep—steady' pattern. Comparison between experiments and simulations reveals that both viscoelastic and viscous models can predict the two steady regions correctly, but only viscoelastic models can simulate the steep increase and decrease of the compressing force. Among the evaluated viscoelastic models, XPP is the most suitable to describe polycarbonate melt compression flow. © 2015 Wiley Periodicals, Inc. J. Appl. Polym. Sci. **2015**, *132*, 42279.

KEYWORDS: polycarbonates; rheology; theory and modeling; viscosity and viscoelasticity

Received 13 November 2014; accepted 19 March 2015

DOI: 10.1002/app.42279

INTRODUCTION

Polycarbonates (PCs) are widely used in transparent industries and most of them are manufactured by injection/compression molding process. Yoon *et al.*[1] found squeeze flow at compression molding reduces the orientation and thus enhances the electrical conductivity. The conventional injection molding has received extensive attention on constitutive models, governing equations, and numerical methods. However, only a few works concerned with squeeze flow can be found in literatures especially for PC. They involve rheological characters, boundary conditions, and numerical methods.

Polymer melt is usually regarded as viscous fluid in squeezing, and sometime is described as generalized Newtonian fluids for small squeezing rates.[2] Juang *et al.*[3] found power-law model fits well with experiments in low temperatures and Carreau model is better for melt temperature above 175°C. Jackson[4] studied squeeze flow of thermoplastic (TP) at high temperature using power-law model. The tests showed the power-law model appears unsuitable for describing the TP viscosity at the very low shear rates, and predicts too small TP thickness reduction for 100–300 kPa pressures, but can be quite accurate for high pressure and high aspect ratios.

However, Pham and Meinecke[5,6] pointed out the squeezed melt undergoes shear deformation at the solid–fluid interface and biaxial extension flow in center region. Only after long squeezing times, when the gap height ratio (R/H) is large, the melt represents predominated shear flow. Only at this time does the melt flow like a power-law fluid subject to a shear flow field. Lee *et al.*[7] showed that elasticity along with inertial effects can become important during start-up of squeezing flow under certain conditions. Debbaut[8] investigated the early development of the squeeze flow for a finite amount of fluid material between two infinite plates using finite element method. He found that the squeezing force decreases with increasing elasticity. Laun[9] established the relationship between recoverable strains in shear and elongation and relaxation time spectrum of melt. He found the linear viscoelastic model can describe the rubber-like behavior at high deformation rate very well, and the single exponential damping function is very good approximation to the highly branched low density polyethylene (LDPE) melt but poor to linear polymers in the Non-Newtonian range. Sherwood[10] pointed out lack of elasticity in constitutive model for squeeze flow that may result in shear stress discrepancy although wall sleep condition is used. Kim and Hyun[11] designed an instrument to measure rheological properties in superposes oscillatory

shear and oscillatory squeeze flow. They found that the normal stress of dynamic helical squeeze flow was hardly influenced by the superposition, the storage and loss moduli showed nonlinear behavior at much lower strain amplitude compared with oscillatory shear flow. Similarly, Cheneler and coworkers[12,13] designed a micro squeeze flow rheometer to measure the rheological behavior of viscoelastic fluid of nano-liter volumes.

Some researchers focused on boundary conditions for squeeze flow during establishing theoretical model. Newtonian and power-law models for squeeze flow with a partial wall slip were reported by Laun *et al.*[14] and Fang *et al.*[15] Their numerical results indicated that the degree of wall slip became more significant as the mold walls got closer, and the slip velocity at the plate increased linearly with the radius up to the rim slip velocity. This phenomenon was also examined by Yang and Zhu[16] for squeeze flow of Bingham fluid with Navier slip condition. The investigation showed that larger slip coefficient produces smaller squeeze force and larger viscosity yields larger squeeze force. Debbaut and Thomas[17] employed multi-mode Giesekus model to predict the periodic force in an oscillatory squeeze flow. They found that inertia correction becomes significant by 10 Hz and is dominant by 100 Hz, and the force for full-slip squeeze-flow is found to be some 200 times smaller than with no-slip. Karapetsas and Tsamopoulos[18] examined the transient squeeze flow of a viscoplastic material between two parallel coaxial discs with mixed finite element method. The study indicated slip condition on the surface of the discs affects the flow field only locally, and the size of the unyielded area decreases significantly as the length of the slip region increases.

Up to now, power-law, Giesecus, Maxwell, and Carreau models for squeezing flow have received considerable consideration.[19] The widely used viscoelastic models such as Leonov,[20] PTT,[21,22] and XPP[23] were seldom investigated. Meanwhile, the well-known viscous model, Cross-WLF,[24] which characterized the shear viscosity of PC well[25,26] was rarely explored for squeeze flow either. Whether they are fit to describe the squeeze rheological behavior have not been evaluated especially for PC. So, we restrict the discussion to the evaluation of these models and find out which one is the most suitable to describe the rheological behavior of polycarbonate squeeze. The squeeze flow model was first established in cylindrical coordinate system with both viscous and viscoelastic models. Then using FDM to simulate flow evolution and predict the compressing force. Finally, the squeeze experiments were carried out to verify the validation of each constitutive model.

SQUEEZE FLOW MODEL

The squeeze flow occurring in between two parallel discs is schematically illustrated in Figure 1. The fluid is compressed and squeezed in between two parallel discs with radius R within the confined time-dependent gap, $h(t)$, either upon the application of a constant force (parallel plate plastometer) or a cross-head moving at a constant velocity ($\dot{h}$). The melt flow is limited within the geometric region: $0 \le r \le R$ and $0 \le z \le h(t)$. Squeeze flows are due to the changing geometry, inherently transient, and inhomogeneous flows.

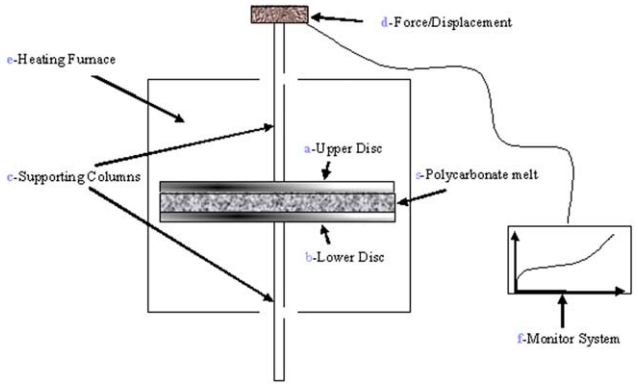

Figure 1. Inner structure of compression part of ARES G2 rheometer. [Color figure can be viewed in the online issue, which is available at wileyonlinelibrary.com.]

Governing Equations

The melt flow within the two discs is axisymmetric, if the gravitational and inertial effects neglected the governing equations for mass and momentum conservation can be written in cylindrical coordinates as

$$\frac{1}{r}\frac{\partial}{\partial r}(rv_r)+\frac{\partial}{\partial z}v_z=0 \tag{1}$$

$$-\frac{\partial p}{\partial r}+\frac{1}{r}\frac{\partial}{\partial r}(r\sigma_{rr})+\frac{\partial}{\partial z}\sigma_{zr}=0 \tag{2}$$

$$-\frac{\partial p}{\partial z}+\frac{1}{r}\frac{\partial}{\partial r}(r\sigma_{rz})+\frac{\partial}{\partial z}\sigma_{zz}=0 \tag{3}$$

where r and z are the radial and axial coordinates, respectively, v_r and v_z are the corresponding velocity components, p is the pressure, and σ_{rr}, σ_{rz}, and σ_{zz} are the stress components.

Boundary Conditions

During squeezing the container keeps open, therefore the pressure at the disc rim can be assumed zero.

$$p=0 \quad \text{at} \quad r=R \tag{4}$$

The flow at the interface between disc and melt is usually governed by slip boundary conditions for generalized Newtonian or low viscous fluid.[14–17] However, the polycarbonate melt is high viscous fluid, it is hard to slip on the wall under low compressing velocity. So the no slip boundary conditions for radial velocity are used on both top and bottom discs.

$$v_r=0, v_z=0 \quad \text{at} \quad z=0 \tag{5}$$

$$v_r=0, v_z=\dot{h} \quad \text{at} \quad z=h \tag{6}$$

Constitutive Equations

For a viscoelastic fluid the stress tensor is expressed as a sum of Newtonian and viscoelastic components:

$$\sigma=\tau_s+\tau_v \tag{7}$$

here τ_v is the extra stress tensor due to viscoelasticity and τ_s is the stress component of a Newtonian fluid given by

$$\boldsymbol{\tau}_s=2\eta_s\dot{\boldsymbol{\gamma}}, \qquad \dot{\boldsymbol{\gamma}}=\left(\nabla\mathbf{v}+\nabla\mathbf{v}^T\right)/2 \tag{8}$$

The extra stress tensor is the sum of different modes

$$\boldsymbol{\tau}_v=\sum_i \boldsymbol{\tau}_i \tag{9}$$

where the stress contribution of the ith mode is given by an appropriate constitutive equation. If the PTT model is applied, the constitutive equation is given by

$$\left[1+\frac{\lambda_i \varepsilon}{\eta_i} tr(\boldsymbol{\tau}_i)\right]\boldsymbol{\tau}_i+\lambda_i \boldsymbol{\tau}\nabla_i=2\eta_i\dot{\gamma}(\mathbf{v}) \tag{10}$$

here ε is the nonlinear parameter, finite value of ε eliminates singularity in extensional viscosity,[27] $tr(\boldsymbol{\tau}_i)$is the trace of the viscoelastic tensor $\boldsymbol{\tau}_i$, and λ_i and η_i are the relaxation time and viscosity of ith mode. In eq. (10) the upper convective derivature is defined as

$$\overset{\nabla}{\boldsymbol{\tau}}_i=\frac{\partial \boldsymbol{\tau}_i}{\partial t}+\mathbf{v}\cdot\nabla\boldsymbol{\tau}_i-\nabla\mathbf{v}\cdot\boldsymbol{\tau}_i-\boldsymbol{\tau}_i\cdot(\nabla\mathbf{v})^T \tag{11}$$

The constitutive equation, eq. (10), for XPP model should be modified as below

$$\boldsymbol{\tau}\nabla_i+\frac{1}{\lambda_{b,i}}\left[\frac{\alpha_i}{G_i}\boldsymbol{\tau}_i\cdot\boldsymbol{\tau}_i+F(\boldsymbol{\tau}_i)\boldsymbol{\tau}_i+G_i(F(\boldsymbol{\tau}_i)-1)\mathbf{I}\right]=2G_i\dot{\gamma}(\mathbf{v}) \tag{12}$$

with

$$F(\boldsymbol{\tau}_i)=2r_i e^{\upsilon_i(\Lambda_i-1)}\left(1-\frac{1}{\Lambda_i}\right)+\frac{1}{\Lambda_i^2}\left[1-\frac{\alpha_i Tr(\boldsymbol{\tau}_i\cdot\boldsymbol{\tau}_i)}{3G_i^2}\right] \tag{13}$$

$$\Lambda_i=\sqrt{1+\frac{Tr(\boldsymbol{\tau}_i)}{3G_i}},\qquad r_i=\frac{\lambda_{b,i}}{\lambda_{s,i}},\qquad \upsilon_i=\frac{2}{q_i},\qquad \lambda_{\mathrm{b,i}}=\lambda_{\mathrm{i}}. \tag{14}$$

In the above equations, G_i is the relaxation modulus, $\lambda_{b,i}$ is the relaxation time of the backbone, $\lambda_{s,i}$ is the relaxation time of q_i arms for the ith mode, α_i is a scalar parameter to control the level of anisotropy, Λ_i is the backbone tube stretch defined as the length of the backbone tube divided by the length at equilibrium, and υ_i is a parameter denoting the influence of the surrounding polymer chains on the backbone tube stretch.

If Leonov model is applied the constitutive equation should be expressed by strain tensor as follow

$$\boldsymbol{\tau}=2\eta_s s\dot{\boldsymbol{\gamma}}+\sum_i\frac{\eta_i}{\lambda_i}\mathbf{C}_i \tag{15}$$

with

$$\overset{\nabla}{\mathbf{C}}_i+\frac{1}{2\lambda_i}(\mathbf{C}_i\cdot\mathbf{C}_i-\mathbf{I})=0,\ \det\mathbf{C}_i=1 \tag{16}$$

where $\mathbf{C}_i$ is the Finger strain tensor of the ith mode, s is the rheological constant, and η_s is the viscosity corresponding to Newtonian fluid and defined as

$$\eta_s\equiv\sum_i\frac{\eta_i}{1-s} \tag{17}$$

This formula indicates the Newtonian effects $\boldsymbol{\tau}=2\eta_s s\dot{\boldsymbol{\gamma}}=\frac{2}{1/s-1}\sum_i\eta_i\dot{\boldsymbol{\gamma}}$ closely depend on the parameter s.

If the elasticity of polymer melt is neglected, the widely used Cross-WLF is the most suitable viscous model

$$\eta(\dot{\gamma},T,p)=\frac{\eta_0(T,p)}{1+\left\{\frac{\eta_0(T,p)}{\tau^*}\dot{\gamma}\right\}^{1-n}} \tag{18}$$

with

$$\eta_0(T,p)=D_1\exp\left\{-\frac{A_1(T-T^*(p))}{\tilde{A}_2+D_3p+(T-T^*(p))}\right\},\ T^*(p)=D_2+D_3p \tag{19}$$

where, n is the power-law index, τ^* is the shear stress level of the asymptotic transition region between the power-law and Newtonian fluids, and A_1, $\tilde{A}_2$, and $D_i(i=1,2,3)$ are material parameters.

NUMERICAL METHOD

In this study, the upper disc keeps constant compressing velocity, $v_z=\dot{h}=\frac{dH}{dt}\equiv const$, thus all the axial velocity v_z at the same level is equal, which indicates $\frac{\partial v_z}{\partial r}=0$. Therefore, substitute eqs. (7–9) into eqs. (2) and (3) yields

$$-\frac{\partial p}{\partial r}+2\eta_s\frac{\partial^2 v_r}{\partial r^2}+\eta_s\frac{\partial^2 v_r}{\partial z^2}+\sum_{i=1}^{M}\left(\frac{\partial\tau_{i,rr}}{\partial r}+\frac{\partial\tau_{i,rz}}{\partial z}\right)=0 \tag{20}$$

$$-\frac{\partial p}{\partial z}+\eta_s\frac{\partial^2 v_r}{\partial r\partial z}+2\eta_s\frac{\partial^2 v_z}{\partial z^2}+\sum_{i=1}^{M}\left(\frac{\partial\tau_{i,rz}}{\partial r}+\frac{\partial\tau_{i,zz}}{\partial z}\right)=0 \tag{21}$$

For Leonov model, the stress component τ_i in eqs. (20) and (21) needs to be replaced by $\frac{\eta_i}{\lambda_i}\mathbf{C}_i$.

The FDM is employed to determine the numerical solution because the polymer flow is restricted within a rectangle region $0\le r\le R; h\le z\le H$, which is suitable for FDM calculation. To keep the numerical consistence and stability, the forward difference and central difference schemes are used to discretize the one order and two order differential terms, respectively, and the 'up-wind' scheme is used to discretize the convect term in constitutive equation. The differential equations corresponding to mass conservative equation [eq. (1)], momentum equations [eqs. (20) and (21)], and constitutive equation [eq. (10)] are discretized as

$$\begin{aligned}&\frac{1}{r_I}\frac{v^n_{r,ij}-v^n_{r,i-1j}}{\Delta r}+v^n_{r,i}+\frac{v^n_{z,ij}-v^n_{z,ij-1}}{\triangle z}=0\\&-\frac{p^n_{ij}-p^n_{i-1j}}{\Delta r}+2\eta_s\frac{v^n_{r,i-1j}-2v^n_{r,ij}+v^n_{r,i+1j}}{\Delta r^2}+\eta_s\frac{v^n_{r,ij-1}-2v^n_{r,ij}+v^n_{r,ij+1}}{\Delta z^2},\end{aligned} \tag{22}$$

$$\begin{aligned}&+\sum_k\left(\frac{\tau^n_{k,rr,ij}-\tau^n_{k,rr,i-1j}}{\Delta r}+\frac{\tau^n_{k,rr,ij}-\tau^n_{k,rz,ij-1}}{\Delta z}\right)=0\\&-\frac{p^n_{ij}-p^n_{ij-1}}{\Delta z}+\eta_s\frac{v^n_{r,i+1j+1}+v^n_{r,i-1j-1}-v^n_{r,i-1j+1}-v^n_{r,i+1j-1}}{\Delta r\Delta z}\\&+2\eta_s\frac{v^n_{zij-1}-2v^n_{zij}+v^n_{zij+1}}{\Delta z^2}\\&+\sum_k\left(\frac{\tau^n_{k,rz,ij}-\tau^n_{k,rz,i-1j}}{\Delta r}+\frac{\tau^n_{k,zz,ij}-\tau^n_{k,zz,ij-1}}{\Delta z}\right)=0\end{aligned} \tag{23}$$

$$\left[1+\frac{\lambda_k\varepsilon}{\eta_k}tr\left(\boldsymbol{\tau}^n_k\right)\right]\boldsymbol{\tau}^n_k+\lambda_k\frac{\boldsymbol{\tau}^n_k-\overset{n-1}{k}}{\Delta t}+\mathbf{v}^{n-1}_{ij}\cdot\begin{pmatrix}\left(\boldsymbol{\tau}^n_{k,ij}-\boldsymbol{\tau}^n_{k,i-1j}\right)/\Delta r\\ \left(\boldsymbol{\tau}^n_{k,ij}-\boldsymbol{\tau}^n_{k,ij-1}\right)/\Delta z\end{pmatrix} \tag{24}$$

AQ14

Table I. Rheological Parameters of 4-Order Viscoelastic Models Measured by Rotating Rheological Experiments

270°C		280°C		290°C		300°C	
Relaxation time λ_i (s)	Modulus G_i (Pa)	Relaxation time λ_i (s)	Modulus G_i (Pa)	Relaxation time λ_i (s)	Modulus G_i (Pa)	Relaxation time λ_i (s)	Modulus G_i (Pa)
5.02923	76.5606	4.73195	51.3094	4.15657	46.913	3.0891	40.0322
0.583092	70.8121	0.22218	108.292	0.41924	50.135	0.363904	42.1809
5.56E-03	81150	9.529E-3	17602.6	5.59E-03	20158.2	8.9702E-3	2983.95
8.56E-04	494619	9.05E-4	398497	6.77E-04	381588	5.8332E-4	218261

$$-\left(\left(\mathbf{v}_{ij}^n-\mathbf{v}_{i-1j}^n\right)/\Delta r \quad \left(\mathbf{v}_{ij}^n-\mathbf{v}_{i-1j}^n\right)/\Delta z\right)\cdot\boldsymbol{\tau}_k^n-\boldsymbol{\tau}_k^n \cdot\begin{pmatrix}\left(\mathbf{v}_{ij}^n-\mathbf{v}_{i-1j}^n\right)/\Delta r\\ \left(\mathbf{v}_{ij}^n-\mathbf{v}_{i-1j}^n\right)/\Delta z\end{pmatrix}=2\eta_k\dot{\gamma}\left(\mathbf{v}_{ij}^{n-1}\right) \tag{25}$$

Combining the above equations subject to boundary conditions [eqs. (4) and (5)] will form the algebraic equations about the unknown pressure p_{ij}^n, velocity $\mathbf{v}_{ij}^n$, and stress $\boldsymbol{\tau}_k^n$. As the stress trace $tr\left(\boldsymbol{\tau}_k^n\right)$ is also unknown, the above algebraic equation is nonlinear and the Newton-Raphson iterative method is used to determine the final solution.

When the unknown variables are determined at every node with above scheme, summate the vertical force at every node of upper disc by the following scheme

$$F_{jk}=\left[p_{jk}+\sum_{i=1}^{M}\left(\tau_{i,rz}+\tau_{i,zz}\right)_{jk}\right] \tag{26}$$

Then integrate the discrete force F_{jk} with bilinear interpolation scheme to get the compressing force imposed on the upper disc.

$$N=\int_{A_{jk}}\int F_{jk}(r,z)\,dA \tag{27}$$

For XPP model, the numerical method is similar to PTT except the nonlinear term discretization. For Leonov model, the unknown variable $\boldsymbol{\tau}_k^n$ needs replaced by strain tensor $\mathbf{C}_k^n$ and subject to additional constraint [eq. (16)].

There are quantitative literatures involved viscous flow simulation and presented good results. Here, we use the conventional method purposed by Chang *et al.*[28] to determine pressure and velocity during squeezing for viscous model.

RESULTS AND DISCUSSION

The experiments were carried out in ARES G2 rheometer of TA Instruments. In this instrument, the upper and lower circular discs (denoted as a and b) are coaxial with same diameter of 25 mm and fixed on the axis c, and the force signal of disc a is collected by the sensor d and displayed on monitor f through A/D converter during compression, see Figure 1. The measured force profile will be used to test the validity of rheological model. In this study, the constant contact area compression mode is applied, so the PC melt is always fully filled within the gap between the two discs. The compression starts from 1.43 mm and stops at 1.0 mm when the external force is removed. During experimenting, the lower disc b is fixed and the upper disc a moves down at constant velocity following with some melt flowing out of the gap. To keep PC melt from absorbing air water, the nitrogen is sweeping the discs constantly.

The rotating rheological experiments were carried out at melt temperatures of 270°C, 280°C, 290°C, and 300°C to get the corresponding relaxation times and moduli listed in Table I. Then using the experimental data to fit the constants of Cross-WLF model as listed in Table II. The squeezing experiments were conducted at four temperatures with compressing speed 0.01 mm/s. These experimental data are used to fit the nonlinear constants in viscoelastic models such as s in Leonov, ε in PTT, and q_i, r_i, α_i in XPP model by trial and error. The fitted constants for Leonov, PTT, and XPP models are summarized in Table III. The validation of the models determined by this method were verified with squeezing experimental results under compressing velocity 0.005 mm/s and 0.02 mm/s at the above four temperatures.

Numerical results were obtained with FDM as depicted in the numerical method section. The velocity, pressure, stress corresponding to different models are determined by solving eqs. (22–26) subjecting to the corresponding boundary conditions. Then integrate the discrete pressure and stress components on z

Table II. Constants of Cross_WLX Model Fitted with the Results of Rotating Rheological Experiments

N	τ^* (Pa)	D_1 (Pa.s)	D_2	D_3 (K/Pa)	A_1	A_2 (K)
0.219	172770	5.24E+14	380.15	0	37.789	51.6

Table III. Constants of Viscoelastic Models Obtained by Best Fitting Squeeze Force

Leonov	PTT	XPP		
S	ϵ	q_i	r_i	α_i
0.00855	0.425	20	2.1	0.8
		2	1.5	0.7
		1	1.6	0.3
		1	7	0.3

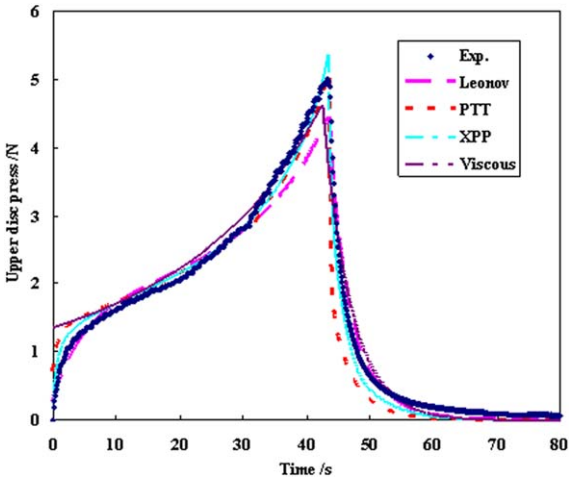

Figure 2. Comparison between experimental data and simulated results at compressing velocity 0.01 mm/s and melt temperature 270°C. [Color figure can be viewed in the online issue, which is available at wileyonlinelibrary.com.]

direction to get compressing force via formula (27) so as to compare with experimental data.

Temperature Effects

Rheological properties such as viscosity, relaxation time closely depend on temperature. It is necessary to verify the models at different temperatures. Figures 2–5 show the measured compressing force at four temperatures increases sharply in start-up stage, then rises steadily to peak value. When the external force imposed on the upper disc withdraws, the compressing force starts to relax. It decreases steeply from the peak to inflexion within 3∼5 s, then goes down slowly to zero. This kind of changing pattern represented by 'steep—steady—steep—steady' can be attributed to the viscoelasticity of polycarbonate melt. In the early compressing stage, the melt elasticity transfers from the top layer to the bottom within short time, leading resistance rising dramatically. In the relaxation stage, the force changes in the opposite direction as the result of the melt elasticity falling

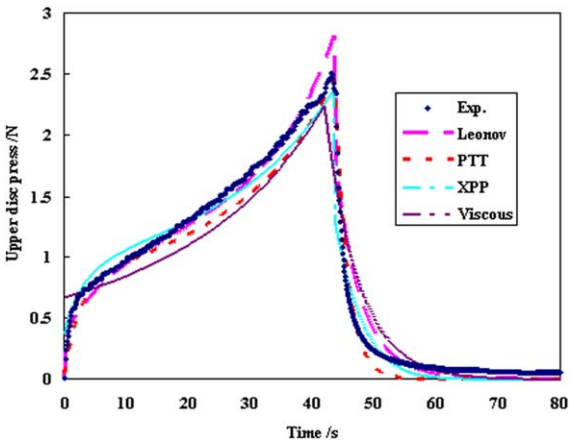

Figure 3. Comparison between experimental data and simulated results at compressing velocity 0.01 mm/s and melt temperature 280°C. [Color figure can be viewed in the online issue, which is available at wileyonlinelibrary.com.]

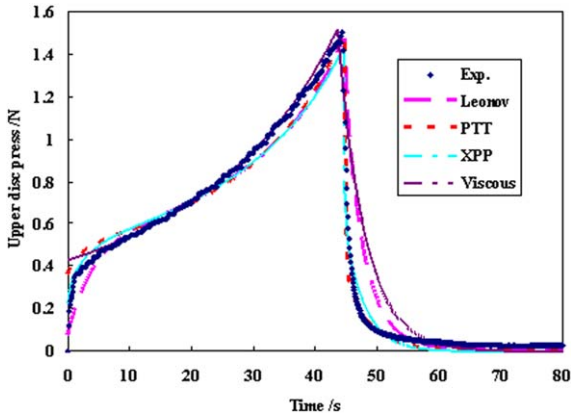

Figure 4. Comparison between experimental data and simulated results at compressing velocity 0.01 mm/s and melt temperature 290°C. [Color figure can be viewed in the online issue, which is available at wileyonlinelibrary.com.]

down quickly from top to bottom. As the stress in viscous model depends on temperature, shear rate, and pressure, and these variables changes smoothly during compressing, so this kind of model cannot predict the sharp increase and decrease change. On the contrary, there exist nonlinear constants in viscoelastic models, which offer the opportunity to adjust the value to better fit the experimental profile. Moreover, time dependent viscoelastic model can store the compressing energy, which leads the simulated force still rises 0.8∼1.2 s after the external force removed rather than decrease at once as viscous model does. So, all the viscoelastic models can predict this force changing pattern correctly, while the viscous model cannot forecast the sharp increase and decrease of compressing force as indicated in Figures 2–5. On the other hand, the melt elasticity decreases as temperature increases, the viscosity plays dominated role for squeezing with high melt temperature, which leads the gross simulated error of viscous model decreases from

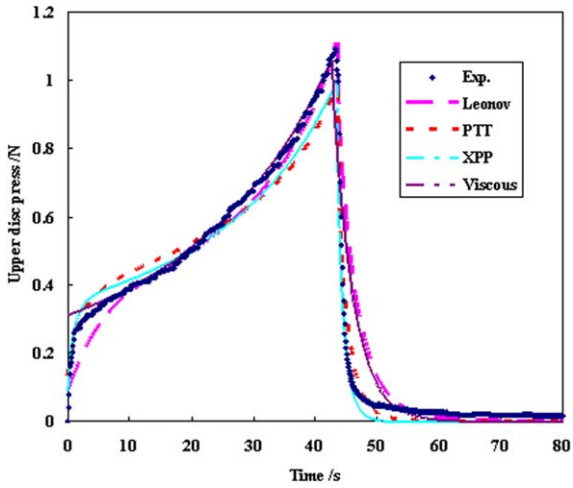

Figure 5. Comparison between experimental data and simulated results at compressing velocity 0.01 mm/s and melt temperature 300°C. [Color figure can be viewed in the online issue, which is available at wileyonlinelibrary.com.]

Table IV. Average Errors and Variances of the Simulated Results from Different Models

	Average error/N				Variance			
Temp.	Leonov	PTT	XPP	Viscous	Leonov	PTT	XPP	Viscous
270°C	0.1474	0.1587	0.1285	0.2043	0.02292	0.07842	0.00887	0.0292
280°C	0.0805	0.0989	0.0743	0.1508	0.00701	0.00301	0.00696	0.0145
290°C	0.0548	0.0391	0.0377	0.0557	0.00728	0.00146	0.00101	0.0113
300°C	0.0375	0.0374	0.0314	0.0434	0.00382	0.00099	0.00081	0.0032

0.2043 at 270°C to 0.0434 at 300°C improved almost four times, see Table IV.

Although all the three viscoelastic models can correctly characterize the PC melt squeeze rheology, the simulated precisions are different. In Leonov model, the stress linearly depends on strain, so its simulated stress cannot increase or decrease abruptly which results in the simulated compressing force less fitting the experimental data in the two 'steep' regions with average error 0.145N higher than other two. However, it works better in the 'steady' regions than other two viscoelastic models as the strain varies smoothly in those regions. As 270°C is approach to the margin of processing temperature, the melt flow is not as smooth as the high temperature melt, after 32 s the measured data starts vibrating and goes up more quickly to the peak value. This character can hardly be captured with ordinary linear model. The PTT model, however, has an additional parameter ε in the nonlinear item to account for the extension effect, so its numerical solution can better approximate to the experimental data in this region, see Figure 2. As there exist 12 parameters in XPP model, which offers more opportunities to control the stress rising or declining rate, nonlinear degree, and elastic effect, so both error and variance indicate XPP model is the best one to characterize the PC melt rheological behavior during squeezing, as illustrated in Figures 2–5 and Table IV.

The nonlinear parameters in viscoelastic models have significant effects on the simulated results. These fitted constants do not vary with temperature, shear rate, and squeezing velocity, so they have different effects on different stages. When the squeeze begins the melt flow starts from upper and gradually transfers to bottom, which indicates the melt flow is restricted within small portion of the gap at the beginning of squeeze, thus the corresponding shear rate is much larger than the following squeeze. Meanwhile, at the end of squeeze the gap becomes much small, but the compressing velocity is same as before, so the shear rate is larger too. Since the constant s in Leonov model represents Newtonian effects dominates for small shear rate, the simulated results in Figures 2–5 shows fair agreement with experimental data of middle squeezing stage and not well for the beginning and end stages. The constant ε in PTT model represents the extension effect which plays obvious role at the beginning squeezing stage, so PTT model can simulate the abrupt increase of compressing force at the onset of squeeze. The nonlinear parameters α_i in XPP model play the similar role as ε in PTT, but more options for these constants makes XPP fit better to experimental data than PTT on the whole.

Compressing Velocity Effects

After the viscoelastic model was established with the parameters obtained under compressing velocity of 0.01 mm/s at four melt temperatures, it needs to be verified with other process

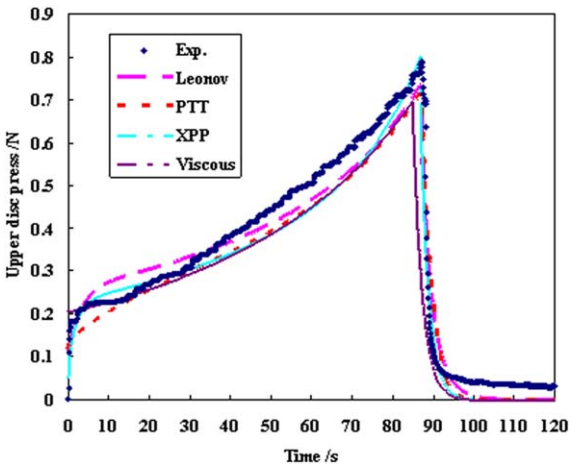

Figure 6. Comparison between experimental data and simulated results at compressing velocity 0.005 mm/s and melt temperature 300°C. [Color figure can be viewed in the online issue, which is available at wileyonlinelibrary.com.]

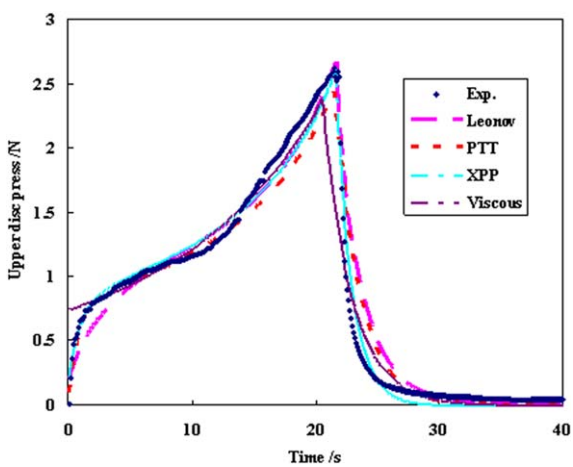

Figure 7. Comparison between experimental data and simulated results at compressing velocity 0.02 mm/s and melt temperature 300°C. [Color figure can be viewed in the online issue, which is available at wileyonlinelibrary.com.]

Table V. Average Errors and Variances of the Simulated Results Under Different Compressing Velocities

	Average error/N				Variance			
Velocity/mm/s	Leonov	PTT	XPP	Viscous	Leonov	PTT	XPP	Viscous
0.005	0.0475	0.0528	0.0426	0.0645	0.00081	0.00051	0.00078	0.0049
0.01	0.0375	0.0374	0.0314	0.0434	0.00382	0.00099	0.00081	0.0032
0.02	0.1074	0.1007	0.0759	0.1343	0.01605	0.01525	0.00379	0.0253

conditions. When the temperature changes, the new rheological parameters such as relaxation time and modulus can be determined with time–temperature equivalent formula, for example, WLF equation. This approach has been proved to be effective both for viscous model and viscoelastic model. Therefore, current study mainly focuses on investigating whether the established models are suitable for different compressing velocities. Here, the experiments with compressing velocity of 0.02 and 0.005 mm/s were performed so as to compare with numerical simulations. Because both experiments and simulations show the similar changing for other temperatures, we just illustrate the rheological behavior at 300°C.

Figures 5–7 shows the compressing force profile corresponding to 0.01 mm/s is the more smooth than the other two. The measured compressing force for 0.005 mm/s vibrates during squeezing, whereas there exist a big inflexion around 12 s for 0.02 mm/s. These results indicate that too slow or too quick compression is not suitable for polycarbonate melt compressing.

Figures 6 and 7 shows both viscous and viscoelastic models can simulate the gross change of compressing force, but viscoelastic model can predict the detailed variation due to the reasons mentioned above. The gross error and variance of XPP model are less than that of Leonov and PTT models, see Table V, implies it is better than the other two viscoelastic models again.

Edge Effect

In this study, the zero pressure is assumed at edge $r=R$ as indicates in eq. (4). This is reasonable at early squeezing stage as only a few polymer melt flows out which cannot accumulates outside the discs. When the squeeze continuous, more melt hangs off and resists the flows, the edge pressure is little high than zero pressure which can affect the normal force applied on the upper disc. Usually this happens when the upper disc gets very close to down disc. At that time the melt flow can be regarded as shear flow as illustrated by Pham and Meinecke.[5] Applying Hele-Shaw model to squeezing governing equations [eqs. (1–3)], the pressure inside the gap can be derived

$$p(r)=p|_{r=R}+\frac{H(R^2-r^2)\dot{h}}{4M\eta\int_0^h\frac{1}{\eta}dz}\ \text{with}\ M=\int_0^h\frac{z^2}{2\eta}dz-\frac{\int_0^h\frac{z}{\eta}dz}{\int_0^h\frac{1}{\eta}dz}\int_0^h\frac{z}{\eta}dz \tag{28}$$

Detail derivation about this formula can be found in appendix A. If the viscosity η is replaced by the average viscosity $\bar{\eta}$ the formula reduces to

$$p(r)=p|_{r=R}+\frac{3\bar{\eta}(R^2-r^2)}{h^3}\dot{h} \tag{29}$$

When the melt accumulates at the edge of the disc, it resists the melt flow and decreases the shear rate, which increases viscosity $\bar{\eta}$. The two terms in the right side of formula (29) are larger than that of zero boundary condition if the edge effect is taken into consideration. Thus, the corresponding simulated pressure and its determined upper disc force will increase.

Figure 2 clearly shows the edge effect of viscous model. The simulated forces are smaller than the measured values during the period of 35 s and 40 s because the zero boundary condition is set in this study. Edge effect is not obvious in Figure 3 as the simulated value is conformably smaller than the experiment data. When melt temperature increases, the viscosity decreases and fluidity increases which leads little melt can accumulates outside the discs, so the edge effect has little influence on final flow of melt temperatures of 290°C and 300°C as indicated in Figures 4 and 5. However, it recovers for compressing velocity of 0.02 mm/s at melt temperature 300°C, see Figure 7, as fast flow leads more melt piles outside discs in short time.

CONCLUSION

This study provides a numerical approach to verify the validation of typical constitutive models. The mathematical model for polycarbonate melt squeeze is established in term of incompressible, viscous or viscoelastic flow in cylinder coordinate system. The FDM is employed to determine the pressure, velocity, and stress in the flow region both for compressing and relaxing stages. The simulated resistant force is obtained by integration of melt pressure and stress at top layer and is used to compare with experimental compressing force. Some special characters from the experimental and simulating results can be summarized as:

1. Due to the viscoelasticity of PC melt the compressing force changes following the pattern of steep—steady—steep—steady rather than the smooth change for generalized Newtonian fluid.
2. The viscous model can predict the compressing force for steady regions but fail to steep regions. If the edge effect is applied, the simulated precision for final compressing will be significantly improved.
3. Viscoelastic model can simulate the force variation well in the whole process if the compressing velocity and melt temperature are correctly specified. Among the evaluated viscoelastic models the XPP model is the most suitable one.

4. The abnormal growth appearing in the profiles of 0.005, 0.02 mm/s compressing velocities and 270°C melt temperatures indicates too slow or quick compression or low temperature is not suitable for PC squeeze.

ACKNOWLEDGMENTS

The financial supports of the National Science Foundation of China (No. 11272291), the Major State Basic Research Development Program of China (973 Program, No.2012CB025900), and Foundation of He'nan Educational Committee (No. 13A460659) for this research work are gratefully acknowledged.

APPENDIX

For thin shear flow, the pressure change on thickness direction can be ignored according to Hele-Shaw theory. The thickness velocity component v_z of each layer keeps constant on radius direction for squeeze flow. Thus the governing equations [eqs. (2) and (3)] for thin squeeze flow can be reduced to

$$-\frac{\partial p}{\partial r}+\frac{\partial}{\partial z}\left(\eta\frac{\partial v_r}{\partial z}\right)=0 \tag{A1}$$

$$\frac{\partial}{\partial z}\left(\eta\frac{\partial v_z}{\partial z}\right)=0 \tag{A2}$$

Double integration on r and z directions respectively subject to boundary conditions yields

$$v_r=\left[\int_0^z\frac{z'}{\eta}dz'-\frac{\int_0^h\frac{z'}{\eta}dz'}{\int_0^h\frac{1}{\eta}dz'}\int_0^z\frac{1}{\eta}dz'\right]\frac{\partial p}{\partial r} \tag{A3}$$

$$v_z=\frac{\int_0^z\frac{1}{\eta}dz'}{\int_0^h\frac{1}{\eta}dz'}\dot{h} \tag{A4}$$

Substitute the two formulae into mass conservative equation [eq. (1)] yields

$$\frac{1}{r}\frac{\partial}{\partial r}\left(r\left(\int_0^z\frac{z'}{\eta}dz'-\frac{\int_0^h\frac{z'}{\eta}dz'}{\int_0^h\frac{1}{\eta}dz'}\int_0^z\frac{1}{\eta}dz'\frac{\partial p}{\partial r}\right)\right)+\frac{1}{\eta\int_0^h\frac{1}{\eta}dz'}\dot{h}=0 \tag{A5}$$

Average the equation on thickness direction

$$\frac{1}{Hr}\frac{\partial}{\partial r}\left(rM\frac{\partial p}{\partial r}\right)+\frac{1}{\eta\int_0^h\frac{1}{\eta}dz}\dot{h}=0 \text{ with } M=\int_0^h\frac{z^2}{2\eta}dz-\frac{\int_0^h\frac{z}{\eta}dz}{\int_0^h\frac{1}{\eta}dz}\int_0^h\frac{z}{\eta}dz \tag{A6}$$

Double integration on r direction again yields the formula of pressure

$$p(r)=p|_{r=R}+\frac{H(R^2-r^2)\dot{h}}{4M\eta\int_0^h\frac{1}{\eta}dz} \tag{A7}$$

REFERENCES

1. Yoon, H.; Okamoto, K.; Umishita, K.; Yamaguchi, M. *Polym. Compos.* **2011**, *32*, 97.
2. Lawal, A.; Kalyon, D. M. *Int. Polymer Process.* **2000**, *1*, 63.
3. Juang, Y.-J.; Lee, L. J.; Koelling, K. W. *Polym. Eng. Sci.* **2002**, *42*, 551.
4. Jackson, P.; Liu, X.-L.; Paton, R. *Compos. Struct.* **2006**, *75*, 179.
5. Pham, H. T.; Meinecke, E. A. *J. Appl. Polym. Sci.* **1994**, *53*, 265.
6. Pham, H. T.; Meinecke, E. A. *J. Appl. Polym. Sci.* **1994**, *53*, 257.
7. Lee, S. J.; Denn, M. M.; Crochet, M. J.; Metzner, A. B.; Riggins, G. J. *J. Non-Newtonian Fluid Mech.* **1984**, *14*, 301.
8. Debbaut, B. *J. Non-Newtonian Fluid Mech.* **2001**, *98*, 15.
9. Laun, H. M. *J. Rheol.* **1986**, *30*(3), 459.
10. Sherwood, J. D. *J. Non-Newtonian Fluid Mech.* **2005**, *129*, 61.
11. Kim, J. H.; Hyun, K. *Rev. Sci. Instrum.* **2012**, *83*, 085105.
12. Cheneler, D.; Bowen, J.; Ward, M. C. L.; Adams, M. J. *Microelectron. Eng.* **2011**, *88*, 1726.
13. Cheneler, D. The design and analysis of a micro squeeze flow rheometer, Ph.D. Thesis, Department of Mechanical Engineering, University of Birmingham, UK, **2010**.
14. Laun, H. M.; Rady, M.; Hassager, O. *J. Non-Newtonian Fluid Mech.* **1999**, *81*, 1.
15. Fang, M.; Gilbert, R. P.; Liu, X.-G. *Math. Comput. Model.* **2010**, *52*, 268.
16. Yang, S.-P.; Zhu, K.-Q. *J. Non-Newtonian Fluid Mech.* **2006**, *138*, 173.
17. Debbaut, B.; Thomas, K. *J. Non-Newtonian Fluid Mech.* **2004**, *124*, 77.
18. Karapetsas, G.; Tsamopoulos, J. *J. Non-Newtonian Fluid Mech.* **2006**, *133*, 35.
19. Engmann, J.; Servais, C.; Burbidge, A. S. *J. Non-Newtonian Fluid Mech.* **2005**, *132*, 1.
20. Leonov, I. *Rheol. Acta* **1976**, *15*, 85.
21. Phan-Thien, N.; Tanner, R. I. *J. Non-Newtonian Fluid Mech.* **1977**, *2*, 353.
22. Phan-Thien, N. *J. Rheol.* **1978**, *22*, 259.
23. Verbeeten, W. M. H.; Peters, G. W. M.; Baaijens, F. P. T. *J. Rheol.* **2001**, *45*(4), 823.
24. Isayev, A. I.; Upadhyay, R. K. Injection and Compression Molding Fundamentals; Marcel Dekker: New York, **1987**.
25. Hsu, C.-L.; Turng, L.-S.; Osswald, T. A.; Rudolph, N.; Dougherty, E.; Gorton, P. *Annu. Tech. Conf. Proc.* **2011**, *2*, 1718.
26. Morizur, J.-F. *Annu. Tech. Conf. Proc.* **2013**, *2*, 1647.
27. Li, J.-M.; Burghardt, W. R.; Yang, B.; Khomami, B. *J. Non-Newtonian Fluid Mech.* **1998**, *74*, 151.
28. Chang, H. H.; Hieber, C. A.; Wang, K. K. *Polym. Eng. Sci.* **1991**, *31*, 116.